GREATER-THAN-ONE RELATIVE PERMEABILITY IN MIXED-WET LIMESTONE

Magali Christensen, Luca Romanello, Yukie Tanino
School of Engineering, University of Aberdeen, UK

This paper was prepared for presentation at the International Symposium of the Society of Core Analysts held in Vienna, Austria, 27 August – 1 September 2017

ABSTRACT

Waterflood relative permeability was measured in Indiana limestone under five mixed-wet conditions, as characterized by macroscopic contact angles on polished calcite which ranged from θ_w = 55° to 150°, and two Darcy velocities: U_w = 1.5 μm/s and 30 μm/s. Oil relative permeability at initial oil saturation decreased and brine relative permeability at residual oil saturation increased with increasing θ_w under the conditions considered presently. Greater-than-one end-point relative permeability was observed at $\theta_w < 90°$ for oil and at $\theta_w > 130^o$ for brine. End-point brine relative permeabilities were larger at the larger U_w under all oil-wet conditions considered, i.e., $\theta_w > 90^\circ$. In contrast to recent literature that associate greater-than-one permeability to the flow of non-wetting fluid against surface, we observed enhanced permeability even when the flowing fluid was the wetting phase. Our results demonstrate that models assuming $k_r \leq 1$ underestimate fluid displacement for a wider range of contact angles than previously documented.

INTRODUCTION

In special core analysis [1, 2], empirical models [3, 4, 5], and pore network simulators [6, 7, 8], it is often assumed that two-phase permeability k_i cannot exceed single-phase permeability k, i.e., $k_{ri} = k_i/k \leq 1$, where k_{ri} is the relative permeability of flowing phase i. However, several laboratory studies report endpoint relative permeability exceeding one [9 and references therein; 10, 11], indicating that, at least under certain conditions, permeability to a fluid is enhanced by the presence of a second phase in the pore space.

In this paper, we consider waterflood relative permeability measurements in mixed-wet Indiana limestone at two of water injection Darcy velocity ranges, U_w = 1.5 - 3.0 and 30 μm/s. We present the dependence of relative permeability on advancing contact angle and identify conditions under which $k_{ri} > 1$.

MATERIALS

Rock

Indiana (USA) limestone cores were used as the porous medium, with a porosity of ϕ = 0.15 and an absolute permeability of k = 6.6 ± 3.1 mD, and of length L = 51.03 ± 0.04 mm or 89.02 ± 0.24 mm. Indiana limestone is 99% calcite and is characterised by a wide pore size distribution [12]. All cores were cleaned by hot Soxhlet extraction with a mixture of methanol and toluene before use.

Fluids

In all experiments, the same aqueous solution of 5 wt.% sodium chloride and 1 wt.% potassium chloride was used as connate and flood water. Five oils were considered: *n*-decane, and 6.6 × 10^{-2} M solutions of cyclohexanecarboxylic acid, cyclohexanepropionic acid, cyclohexanebutyric acid, and cyclohexanepentanoic acid in *n*-decane. These organic acids, of similar molecular structure but different alkyl chain lengths, alter the wettability of calcite in order of increasing alkyl chain length (Fig. 1), resulting in dynamic advancing contact angles of θ_w = 55º, 110º, 125º, 135º, and 150º [13]. Interfacial tension for the fluid pairs considered, σ, can be found in Ref. [13].

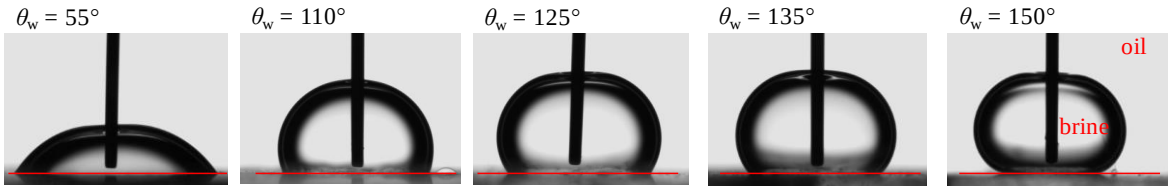

Figure 1. A drop of brine advancing on a polished calcite substrate submerged in, from left to right, *n*-decane and 6.6 × 10^{-2} M solutions of cyclohexanecarboxylic acid, cyclohexanepropionic acid, cyclohexanebutyric acid, and cyclohexanepentanoic acid in *n*-decane.

DISPLACEMENT EXPERIMENTS

Two sets of unsteady state relative permeability experiments were performed: one at low waterflood injection velocity [14] and one at high velocity [15].

Low Waterflood Velocity

Details of the coreflood apparatus and procedure can be found in Refs. [12, 13, 16]. The key steps were as follows [13]:

1. Each core was alternately evacuated and flushed with gaseous CO_2 to remove air, then flushed with degassed brine to fully saturate it. k was measured.
2. The test oil was injected into the core at constant pressure to establish initial oil saturation, S_{oi}, using the porous plate method.
3. Permeability to oil at initial oil saturation, $k_o(S_{oi})$, was measured.

4. Up to 100 pore volumes (pv) of degassed brine was injected at constant Darcy velocity of $U_w = 1.5\ \mu$m/s.

Core-averaged S_{oi} and S_{or} were measured by mass balance. The corresponding microscopic waterflood capillary number,

$$\mathrm{Ca} = \frac{\mu_w U_w}{\sigma}, \tag{1}$$

where μ_w is the dynamic viscosity of the brine, varied between Ca = 3.1×10^{-8} and 9.7×10^{-8}, indicating that flow rates remained below the capillary desaturation threshold.

High Waterflood Velocity

Details of the coreflood apparatus and procedure can be found in Ref. [15]. The key steps are as follows:

1. Each core was evacuated for 24 hours to remove air. The core was then saturated with the equivalent of 60 pv of brine before k was measured.
2. Primary drainage was completed in two stages. First, Blandol was injected in the core at constant flow rate increased in discrete intervals. Second, 10 to 20 pv of the test oil were injected at constant flow rate until Blandol production ceased. The cores were left to age in the test oil for an average of 8 hours.
3. Brine was injected at constant rate of $U_w = 30\ \mu$m/s until oil production and the pressure drop across the length of the core approached steady state (Fig. 2).

The waterflood rate corresponds to Ca = $(1 - 2) \times 10^{-6}$. Pressure drop and effluent production was monitored throughout the waterflood, and core-averaged saturation was determined volumetrically.

k and $k_o(S_{oi})$ were calculated using the pressure drop across the core at steady state at constant flow rate as

$$k_i = \mu_i \frac{U_i}{\Delta P_i / L}, \tag{2}$$

where μ_i and U_i are the viscosity and Darcy velocity of the injected fluid i, and ΔP_i is the pressure drop across the core. In particular, $k_o(S_{oi})$ was calculated by measuring ΔP_i for a constant oil injection rate of $U_o = 60\ \mu$m/s [Ca = $(1.6 – 3.2) \times 10^{-6}$].

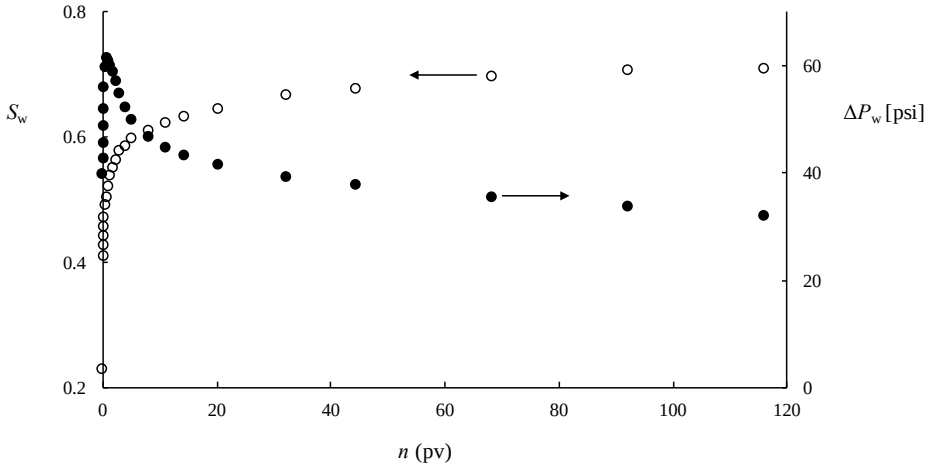

Figure 2. Brine saturation (open circles) and ΔP_w (solid circles) during waterflood as a function of the cumulative number of pore volumes of brine injected for $U_w = 30$ μm/s, $\theta_w = 150°$.

Relative permeability determination

Relative permeabilities to oil k_{ro} and brine k_{rw} during waterflood were determined by iterative history matching of simulated ΔP_w after water breakthrough to measured values using software CYDAR™ (CYDAREX). First, waterflood (secondary imbibition) capillary pressure curves, $P_c^B(S_w)$, of a Berea sandstone pore network from Ref. [12] were predicted for each oil/brine combination using a two-phase pore network simulator developed by Valvatne & Blunt [6]; details of the pore network are available in Ref. [12]. To account for differences in S_{or}, water saturation was rescaled as

$$\hat{S}_w(t) = \frac{S_w(t) - (1 - S_{oi})}{S_{oi} - S_{or}} \tag{3}$$

Similarly, P_c^B was scaled using the Leverett-J function, i.e.,

$$P_c(\hat{S}_w) = P_c^B(\hat{S}_w)\sqrt{\frac{k^B/\phi^B}{k/\phi}} \quad , \tag{4}$$

where superscript B denotes properties of the Berea sandstone pore network. Brooks-Corey functions were used as input relative permeability curves [17]

$$k_{rw} = k_{rw}(S_{or})\,\hat{S}_w^{\alpha_w} \quad , \quad k_{ro} = k_{ro}(S_{oi})\,(1-\hat{S}_w)^{\alpha_o} \quad , \tag{5}$$

where α_w, α_o, $k_{ro}(S_{oi})$, and $k_{rw}(S_{or})$ were fitting parameters whose values were determined by matching ΔP_w predicted by the simulator to measured values in the least squares sense after water breakthrough (e.g., Fig. 3).

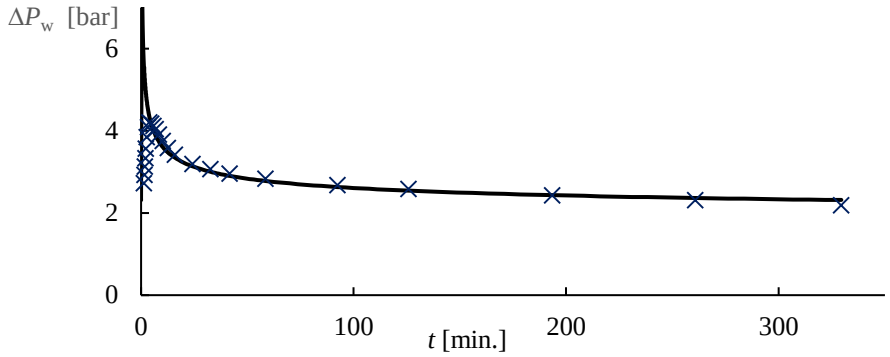

Figure 3. Measured (markers) and simulated (solid line) pressure drop across the length of the core. U_w = 30 μm/s; θ_w = 150°.

RESULTS

Figure 4 presents best-fit Brooks–Corey functions for k_{rw} and k_{ro} at θ_w = 110˚, 135˚, and 150˚ for Ca ~ 10^{-6} (solid lines) and for Ca ~ (3 to 10) × 10^{-8} (dashed). $k_{ro}(S_{oi})$ does not differ between the two Ca considered, but $k_{rw}(S_{or})$ is up to a factor of 3larger at the larger Ca. $k_{ro}(S_{oi}) \lesssim 1$ for $\theta_w > 90$˚, which is consistent with previous measurements in the literature for mixed-wet oil/brine/rock systems [20]. In contrast, $k_{rw} > 1$ at θ_w = 135˚ and 150˚ for large Ca at $S_w \gtrsim 0.6$ and $S_w \gtrsim 0.5$, respectively, suggesting that greater-than-one relative permeability may be a common state for mixed-wet oil/brine/rock systems.

Table 1. Summary of relative permeability measurements completed at U_w = 1.5 μm/s Corefloods are a subset of those reported in Ref. [14].

						best-fit parameters				
θ_w [˚]	**core**	ϕ	L [mm]	k [mD]	S_{oi}	S_{or}	$k_{ro}(S_{oi})$	$k_{rw}(S_{or})$	α_w	α_o
55	M	0.15	89.02	8.8	0.86	0.37	1.40	0.11	1.9	1
110	W	0.15	88.97	6.3	0.88	0.25	0.90	0.40	1	2.6
125	O	0.14	88.50	3.8	0.89	0.32	1.10	0.56	1.1	2.8
135	AD	0.14	89.60	2.0	0.88	0.31	0.98	0.49	1.1	5
150	N	0.15	89.12	11.1	0.82	0.10	0.63	0.58	1.2	2.4

Table 2. Summary of relative permeability measurements completed at U_w = 30 μm/s.

					best-fit parameters				
θ_w [˚]	ϕ	L [mm]	k [mD]	S_{oi}	S_{or}	$k_{ro}(S_{oi})$	$k_{rw}(S_{or})$	α_w	α_o
110	0.15	51.07	7.4	0.81	0.08	0.83	0.52	3.5	2.9
135	0.14	51.05	3.6	0.82	0.35	0.96	1.4	3.4	3.0
150	0.15	50.98	9.2	0.77	0.48	0.65	1.3	5.9	2.3

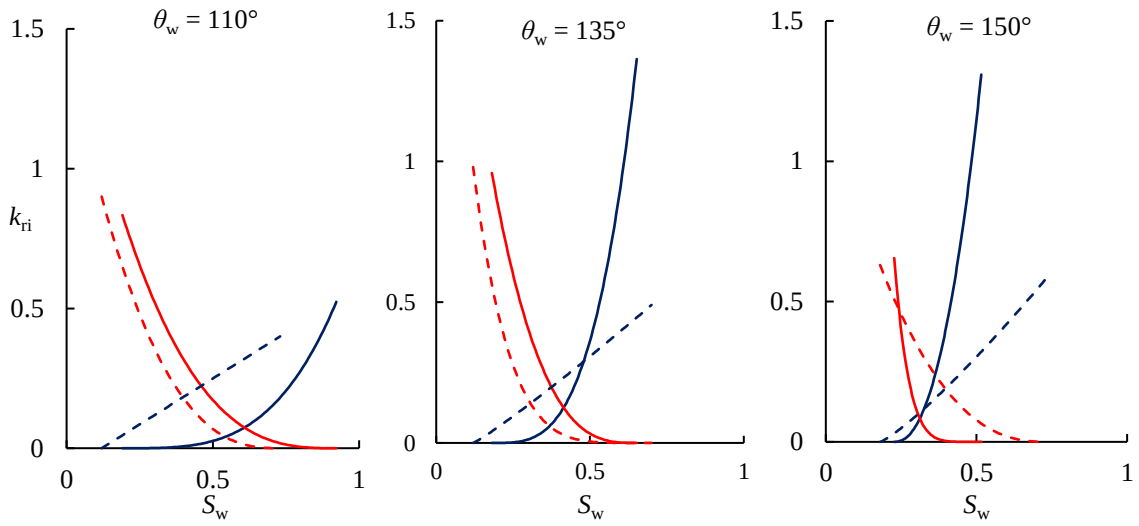

Figure 4. Best-fit Brooks-Corey functions for oil (red) and brine (blue) relative permeabilities [Eq. (5)] for U_w = 1.5 μm/s (dashed lines) and U_w = 30 μm/s (solid lines).

Permeability Enhancement

Consider a bundle of N identical, parallel capillary tubes of uniform radius r_p and length L distributed over a bulk cross-sectional area A; the bundle represents the rock and individual tubes represent pore channels spanning the length of the rock [21]. The porosity of the bundle is $\phi = (N\pi r_p^2)/A$. Flow in each tube is described by the Hagen-Poiseuille equation,

$$\mu \frac{U_p}{\Delta P/L} = \frac{r_p^2}{8}, \tag{6}$$

where ΔP is the constant applied pressure drop, U_p is the resulting mean velocity within each tube, and subscript p denotes properties of a single pore channel (capillary tube). The left-hand-side of Eq. (6) is, by definition [Eq. (2)], the permeability of each tube, and $k_p = r_p^2/8$.

If the bundle contains a single phase, the net volumetric flux through the bundle is $U_p A_{eff}$ and the corresponding Darcy velocity is $U = U_p A_{eff}/A$ where $A_{eff} = N\pi r_p^2 = \pi A$ is the net cross-sectional area through which the fluid flows. It then follows that the permeability of the bundle, $k = \mu/(\Delta P/L)$, is related to the permeability of a single capillary tube as $k = k_p A_{eff}/A = k_p \phi$.

Next, consider a bundle containing two phases, where only one phase i is continuous and flowing. This scenario is equivalent to only N_c ($\leq N$) of the N tubes conducting fluid. Here, the net cross-sectional area conducting fluid is $A_{eff} = N_c \pi r_p^2 = (N_c/N)\, \phi A$. Finally, a non-conducting tube represents pore space occupied by the non-flowing phase j in the present experiments and,

accordingly, 1-$N_c/N = S_j$. The relative permeability of the flowing phase is thus given by

$$k_{ri} = \frac{k_p(1\text{-}S_j)\phi}{k_p\phi} = 1 - S_j = S_i. \quad (7)$$

Figure 5 presents end-point relative permeabilities, $k_{rw}(S_{or})$ and $k_{ro}(S_{oi})$, normalised by the respective saturations as a function of θ_w and the corresponding contact angle measured through the oil phase θ_o ($\equiv 180° - \theta_w$), respectively. From Eq. (7), $k_{ri}/S_i > 1$ indicates permeability enhancement correcting for the impact of reduced cross-sectional area available to flow due to the presence of the residual phase. k_{ri}/S_i increases with increasing θ_i for both phases, i.e., relative permeability increases as the grains become increasingly non-wetting towards the flowing phase. $k_{ro}(S_{oi})/S_{oi}$ does not differ between the two U_w considered, and $k_{ro}(S_{oi})/S_{oi} > 1$ for $\theta_o \geq 45°$ at both flow rates, indicating that enhanced permeability can occur even when the flowing phase is the wetting phase. In contrast, $k_{rw}(S_{or})/(1\text{-}S_{or}) > 1$ only at $\theta_w > 130°$, i.e., when brine is the non-wetting phase.

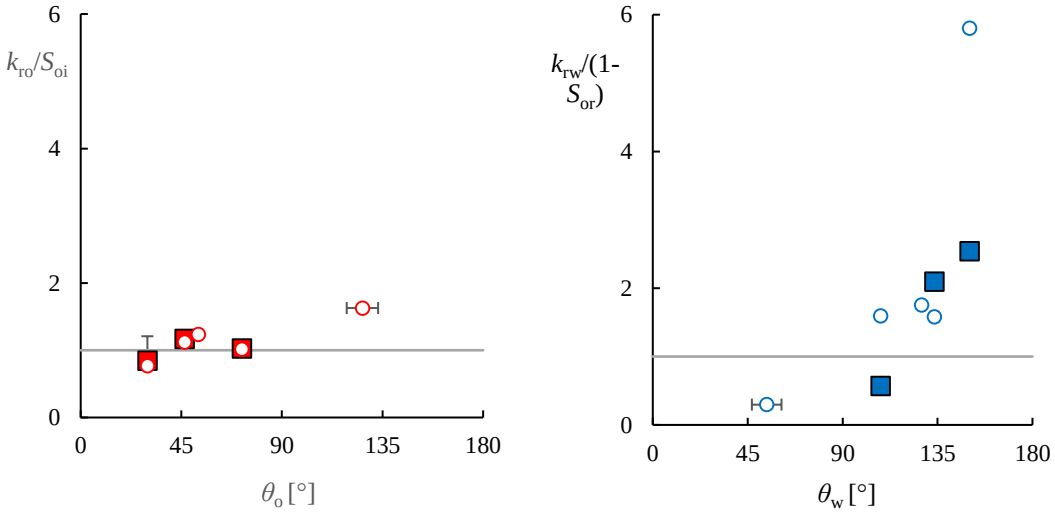

Figure 5. End-point relative permeability normalised by the saturation of the flowing phase as a function of the contact angle θ_i measured through the flowing phase i. U_w = 30 μm/s (solid squares) and U_w = 1.5 μm/s (open circles). Horizontal bars are standard errors of the mean. Vertical bar on (θ_o, k_{ro}/S_{oi}) = (30°, 0.85) depicts the disagreement between $k_{ro}(S_{oi})$ calculated using Eq. (2) and that in the best-fit Brooks-Corey function.

CONCLUSIONS

We present $k_r(S_w)$ curves for in Indiana limestone under different mixed wettability conditions. In addition, we compare end point brine and oil relative permeabilities to measurements completed at lower capillary numbers [14]. Relative oil and brine permeabilities decrease and increase, respectively, as θ_w increases, i.e., as the grains become increasingly non-wetting to the

flowing phase. Greater-than-one end-point relative permeability was observed at $\theta_w < 90°$ for oil and at $\theta_w > 130^o$ for brine. In contrast to recent literature that associate enhanced permeability to the flow of non-wetting fluid against a solid surface, we observe enhanced permeability even when the flowing fluid was the wetting phase.

ACKNOWLEDGEMENTS

This material contains work supported by a Society of Petrophysicists and Well Log Analysts Foundation grant and an Aberdeen Formation Evaluation Society scholarship. MC was supported by the University of Aberdeen College of Physical Sciences studentship. The high velocity waterfloods were performed at Corex (UK) Ltd.; the authors gratefully acknowledge Corex (UK) Ltd. for allowing LR access to their laboratory facilities during his work-based placement. The contact angle measurements were performed at the Max Planck Institute for Dynamics and Self-Organization, Germany. The authors thank Amer Syed for his assistance with the assembly and maintenance of the coreflood rigs, Guillaume Lenormand at CYDAREX for helpful suggestions on their software CYDAR™, and reviewer Arjen Cense for his insightful comments and suggestions.

REFERENCES

1. Jerauld, G. (1997) Prudhoe bay gas/oil relative permeability, *SPE Res. Eng.*, 12(1), 66–73, doi:10.2118/35718-PA.
2. Al-Gharbi, M. S., X. Jing, M. Kraaijveld, J. B. Hognestad & P. O. Udeh (2007) SCAL relative permeability measurements and analyses for a cluster of fields in South Oman, in *Proc.*, International Petroleum Technology Conference, 4-6 Dec., International Petroleum Technology Conference, Dubai, UAE.
3. Honarpour, M., L. F. Koederitz & A. H. Harvey (1982) Empirical equations for estimating two-phase relative permeability in consolidated rock, *J. Petrol. Technol.*, 34(12), 2905–2908, doi:10.2118/9966-PA.
4. Burdine, N. T. (1953) Relative permeability calculations from pore size distribution data, *J. Petrol. Technol.*, 5(3), 71–78, doi:10.2118/225-G.
5. Lomeland, F., E. Ebeltoft & W. H. Thomas (2005) A new versatile relative permeability correlation, in *Proc.*, International Symposium of the Society of Core Analysts, 21-25 Aug., SCA2005-32, Toronto, Canada.
6. Valvatne, P. H. & M. J. Blunt (2004) Predictive pore-scale modeling of two-phase flow in mixed-wet media, *Water Resour. Res.*, 40(7), W07,406, doi:10.1029/2003WR002627.
7. Joekar-Niasar, V., S. M. Hassanizadeh & A. Leijnse (2008) Insights into the relationships among capillary pressure, saturation, interfacial area and relative

permeability using pore-network modeling, *Transp. Porous Med.*, 74(2), 201–219, doi:10.1007/s11242- 007-9191-7.

8. Ryazanov, A. V., M. I. J. van Dijke & K. S. Sorbie (2010) Pore-network prediction of residual oil saturation based on oil layer drainage in mixed-wet systems, in *Proc.*, SPE Improved Oil Recovery Symposium, 24-28 April, Society of Petroleum Engineers, Oklahoma, USA, doi:10.2118/129919-MS.
9. Berg, S., A. W. Cense, J. P. Hofman & R. M. M. Smits (2008) Two-phase flow in porous media with slip boundary condition, *Transport Porous Med.*, 74(3), 275–292.
10. Nowak, T. & R. Krueger (1951) The effect of mud filtrates and mud particles upon the permeabilities of cores, in *Drilling and Production Practice*, American Petroleum Institute.
11. Morrow, N. R., P. J. Cram & F. McCaffery (1973) Displacement studies in dolomite with wettability control by octanoic acid, *Soc. Petrol. Eng. J.*, 13(4), 221–232, doi: 10.2118/3993-PA.
12. Tanino, Y. & M. J. Blunt (2012) Capillary trapping in sandstones and carbonates: Dependence on pore structure, *Water Resour. Res.*, 48(8), doi:10.1029/2011WR011712.
13. Christensen, M. & Y. Tanino (2017) Waterflood oil recovery from mixed-wet limestone: dependence on contact angle, *Energy Fuel*, 31(2), 1529–1535, doi: 10.1021/acs.energyfuels.6b03249.
14. Christensen, M. & Y. Tanino (2017) Enhanced permeability due to apparent oil/brine slippage in limestone and its dependence on wettability, *Geophys. Res. Lett.*, doi: 10.1002/2017GL073603
15. Romanello, L. (2015) Impact of wettability on relative permeability, MSc thesis, University of Aberdeen.
16. Tanino, Y. & M. J. Blunt (2013) Laboratory investigation of capillary trapping under mixed-wet conditions, *Water Resour. Res.*, 49(7), 4311–4319, doi:10.1002/wrcr.20344.
17. Corey, A. T. (1954) The interrelation between gas and oil relative permeabilities, *Producers Monthly*, 19(1), 38–41.
18. Tie, H. & Morrow, N. R. (2005) Low-flood-rate residual saturations in carbonate rocks. *Proc*., International Petroleum Technology Conference, 21-23 Nov., Doha, Qatar.
19. Tanino, Y., B. Akamairo, M. Christensen & S. A. Bowden (2015) Impact of displacement rate on waterflood oil recovery under mixed-wet conditions, in *Proc.*, International Symposium of the Society of Core Analysts, SCA-A031, St. John's Newfoundland and Labrador, Canada.
20. Owens, W. W. & D. L. Archer (1971) The effect of rock wettability on oil-water relative permeability relationships, *J. Petrol. Technol*., 23(7), 873–878, doi:10.2118/3034-PA.
21. Dullien, F. A. L. (1991) *Porous Media. Fluid Transport and Pore Structure*, 2nd ed., Academic San Diego, Calif.